Journal of Hazardous Materials 424 (2022) 127337

Contents lists available at ScienceDirect

Journal of Hazardous Materials

journal homepage: www.elsevier.com/locate/jhazmat

Catalytic stability enhancement for pollutant removal via balancing lattice oxygen mobility and VOCs adsorption

Yuan Feng [a], Chongchen Wang [b], Can Wang [c], Haibao Huang [d], Hsing-Cheng Hsi [e], Erhong Duan [f], Yuxi Liu [a], Guangsheng Guo [a], Hongxing Dai [a], Jiguang Deng [a,*]

[a] Key Laboratory of Beijing on Regional Air Pollution Control, Beijing Key Laboratory for Green Catalysis and Separation, Center of Excellence for Environmental Safety and Biological Effects, Beijing University of Technology, Beijing 100124, China
[b] Beijing Key Laboratory of Functional Materials for Building Structure and Environment Remediation, Beijing University of Civil Engineering and Architecture, Beijing 100044, China
[c] School of Environmental Science and Engineering, Tianjin University, Tianjin 300350, China
[d] School of Environmental Science and Engineering, Sun Yat-Sen University, Guangzhou 510275, China
[e] Graduate Institute of Environmental Engineering, National Taiwan University, Taipei 10617, Taiwan, ROC
[f] School of Environmental Science and Engineering, Hebei University of Science and Technology, 26th Yuxiang Street, Shijiazhuang, Hebei 050018, China

ARTICLE INFO

Keywords:
VOCs removal
Single atom catalyst
Catalytic stability
Lattice oxygen mobility
VOCs adsorption

ABSTRACT

Manganese oxide supported Pt single atoms (Pt_1/MnO_x) are prepared by the molten salt method. Catalytic oxidation of toluene and *iso*-hexane, typical emissions from furniture paints industry, is tested. Pt_1/MnO_x shows poor and high catalytic stability for toluene and *iso*-hexane oxidation, respectively. Enhancement in the catalytic stability for toluene oxidation is observed after the hydrogen reduction treatment of Pt_1/MnO_x at 200 °C. The hydrogen treated catalyst possesses the weaker Mn–O bonds and lower coordination number of Pt—O, with superior mobility of lattice oxygen and appropriate toluene adsorption. Balancing lattice oxygen mobility and volatile organic compounds adsorption is important for the catalytic stability of Pt_1/MnO_x. For the oxidation of toluene and *iso*-hexane mixture, owing to the competitive adsorption, *iso*-hexane oxidation is greatly inhibited, while toluene oxidation is not influenced. The present Pt_1/MnO_x catalyst holds promising prospect in furniture paints industry applications because of high catalytic stability and water resistance ability.

1. Introduction

With the rapid development of industrial, air pollution has become one of the major environmental challenges. Volatile organic compounds (VOCs), as a typical kind of air pollutant, are an important factor influencing air quality and human health (Li et al., 2019; Ribeiro et al., 2019). The industrial sector still accounts for a large proportion among the VOCs emission sources (Yuan et al., 2013; Zhu et al., 2020). Catalytic oxidation is currently one of the effective pathways for completely eliminating VOCs emitted from industry.

Alkanes and aromatic hydrocarbons are the main pollutants as solvents for furniture paints industry. Toluene and *iso*-hexane together account for about half of the total emissions (Zheng et al., 2013). Although toluene oxidation has been widely investigated, up to now, little work has been done about the catalytic oxidation of VOCs mixture. The previous work reveals the complexity of the processes that take place during oxidation of VOCs mixture (Ma et al., 2021; Wang et al., 2020b). For example, benzene oxidation activity is strongly suppressed in the presence of ethyl acetate over the Pt/TiO_2 (W^{6+}) catalyst (Papaefthimiou et al., 1998), and during oxidation of benzene—butanol mixture, benzene oxidation is completely suppressed as long as butanol is present (Papaefthimiou et al., 1997). Meanwhile, the water tolerance of the catalyst should be considered due to the unavoidable co-presence of water in the feed gas (Cao et al., 2019; Feng et al., 2021; Li et al., 2020).

The isolated single atoms (ISAS) catalyst greatly improves atom utilization, which is approaching almost 100%, and has been widely used for various applications (e.g., selective hydrogenation (Zhang et al., 2017), CO oxidation (Qiao et al., 2011), water-gas shift reaction (Yang et al., 2015)). Noble metal based ISAS catalysts are commonly prepared by the precipitation, impregnation or high-temperature pyrolysis methods (Qiao et al., 2015; Y.H. Zhang et al., 2018; J. Zhang et al., 2018;

* Corresponding author.
E-mail address: jgdeng@bjut.edu.cn (J. Deng).

https://doi.org/10.1016/j.jhazmat.2021.127337
Received 31 July 2021; Received in revised form 18 September 2021; Accepted 21 September 2021
Available online 25 September 2021

Yin et al., 2016). However, these methods require multi-step reactions, which are hardly applicable for large-scale industry. Low-cost molten salts, as reaction medium, exhibit much lower melting temperature, important dissolution capacities, and higher ion migration rates, making the molten salt method quite simple and well controlled (Gao et al., 2021; Voisin et al., 2020). Previously, we prepared the Ag/Mn_2O_3 catalysts via the in situ molten salt strategy, which exhibited better catalytic performance for toluene oxidation than the counterparts derived via the other preparation methods (Deng et al., 2015). To the best of our knowledge, there have been so far no reports on the catalytic removal of VOCs using the supported single-atom Pt catalysts prepared by the in situ molten salt method.

In the present work, a molten salt method is designed to synthesize Pt_1 atoms anchored on MnO_x nanowires catalyst. The structural properties and surface behaviors are characterized by various techniques, to understand the effect of VOCs adsorption and oxygen mobility on the catalytic performance of the as-obtained samples for VOCs (toluene and *iso*-hexane) oxidation. It is found that single-atom catalyst treated in H_2 exhibits an excellent catalytic activity and stability, particularly in the presence of water.

2. Experiment

2.1. Catalyst preparation

$NaNO_3$ (99.0%) and $MnSO_4$ (99.0%) are purchased from Sinopharm Group Chemical Reagent Co., Ltd. NaF (99.0%) and Tetraammineplatinum (II) nitrate (Pt≥50%) is purchased from Innochem Chemical Reagent Co., Ltd. All the agents are analytical grade or better and used directly without further purification.

MnO_x nanowires is prepared by the molten salt method as described in our earlier works (Deng et al., 2015; Zhang et al., 2019). 29.4 g of $NaNO_3$, 0.6 g of NaF, and 1.0 g of $MnSO_4$ are first well ground after ball milling for 15 min. The mixture is calcined for 2 h in a muffle furnace at 380 °C with a ramp of 1 °C/min. The MnO_x nanowires are obtained after filtration, washing with deionized water and ethanol for inorganic salt (Na^+, F^- and Cl^- ions) removal, and drying at 70 °C overnight in an oven.

An aqueous solution of tetraammineplatinum (II) nitrate (540 μL, 0.01 mol/L) is added into the solid mixture of 0.6 g NaF, 29.4 g $NaNO_3$ and 1.0 g $MnSO_4$, and the wet powder is dried at 70 °C overnight. The mixture is well ground for 15 min in a ball mill, and then calcined at 380 °C for 2 h in a muffle furnace. After washing, the obtained material is dried at 70 °C overnight. Before the characterization and catalytic performance evaluation, the 0.16 wt% Pt/MnO_x sample is pretreated at 200 °C in an O_2 flow (20 mL/min) for 1 h, and the as-obtained sample is denoted as Pt_1/MnO_x. The actual Pt loading of Pt_1/MnO_x is 0.16 wt% obtained by the inductively coupled plasma atomic emission spectroscopic (ICP—AES) method. In addition, the 0.16 wt% Pt_1/MnO_x samples treated in a flow of 10% H_2/He (50 mL/min) at 150 °C and 200 °C for 2 h is denoted as H_2-Pt_1/MnO_x-150 and H_2-Pt_1/MnO_x-200, respectively. In the present study, 0.033 wt% and 0.55 wt% Pt_1/MnO_x are also prepared for the initial screening.

2.2. Catalyst characterization

The present catalysts are characterized by various techniques. Crystal structures are characterized by the X-ray diffraction (XRD) technique on a Bruker/AXS D8 Advance diffractometer, with Cu Kα radiation and nickel filter (λ = 0.154 nm). Surface areas are determined using the BET (Brunauer—Emmett—Teller) method via N_2 adsorption at —196 °C on a Micromeritics ASAP 2020 analyzer. All of the samples are degassed at 200 °C for 2 h under vacuum prior to measurement. X-ray photoelectron spectroscopy (XPS) is used to determine the O 1s and C 1s binding energies (BEs) of the surface species with Mg Kα (hν = 1253.6 eV) as the excitation source. The C 1s signal at 284.6 eV is taken as reference for BE calibration. The Pt L-edge spectra are acquired at beamline 1W1B of the Beijing Synchrotron Radiation Facilities. Scanning electron microscopic (SEM) images are recorded on a Gemini Zeiss Supra 55 apparatus (operating at 10 kV). Transmission electron microscopic (TEM) images are recorded using a FEI G2 80–200 instrument with B–U EDAX spectrometer. High resolution—STEM and the EDS measurements are performed on an atomic resolution analytical microscope (JEM-ARM 200 F) operating at 200 kV. The Fourier transform infrared (FT-IR) spectra are recorded with a resolution of 4 cm^{-1} on a Bruker Tensor II spectrometer. *In situ* diffuse reflectance Fourier transform infrared spectroscopic (DRIFT) experiments are carried on a Nicolet 6700 FT-IR spectrometer with a liquid nitrogen-cooling MCT detector. Before the in situ DRIFT experiment, 30 mg of the sample is loaded into an IR cell with KBr windows. Subsequently, the sample is cooled to 30 °C and purged with a N_2 flow of 20 mL/min for 30 min before the background spectrum is recorded. Finally, the catalysts are exposed to a 10% CO/He with the flow of 20 mL/min. Hydrogen temperature-programmed reduction (H_2—TPR) experiments are carried out on a chemical adsorption analyzer (Autochem II 2920, Micromeritics). Before TPR measurement, ca. 30 mg of the sample (40–60 mesh) is loaded to a quartz fixed-bed U-shaped microreactor (i.d. = 4 mm) and pretreated in a 20 vol% O_2/He flow of 30 mL/min at 250 °C for 1 h. After being cooled to RT at the same atmosphere, the sample is purged in a He flow of 30 mL/min for 15 min. The pretreated sample is exposed to a flow (50 mL/min) of 10% H_2/He mixture and heated from 50 °C to 800 °C at a ramp of 10 °C/min. The alteration in H_2 concentration of the effluent is monitored online by the chemical adsorption analyzer. Temperature programmed desorption of oxygen (O_2—TPD) is carried out on the apparatus same as that used in the H_2—TPR experiments. The samples (30 mg) are first treated at 250 °C for 1 h in an O_2 flow of 30 mL/min and cooled to room temperature in the same atmosphere, and kept in the same flow for 1 h. Before the sample is heated from 50 °C to 800 °C at a ramp of 10 °C/min, a helium flow of 30 mL/min is employed to remove the O_2 for 30 min. The oxygen concentration in the effluent is continuously monitored by the online Mass Spectrometry. The metal dispersion is measured using chemisorption method (AutoChem II 2920, Micromeritics). The sample is reduced in a H_2 flow (30 mL/min) at 100 °C for 2 h, purged with a He flow (30 mL/min) for 1 h and cooled to 50 °C. Then, it is saturated with pulses of CO. The uptake of CO during the chemisorption is measured by a TCD. VOCs—temperature programed desorption (VOCs—TPD) and temperature—programmed surface reaction of toluene (toluene—TPSR) experiments are performed in a quartz U-shaped tube. Prior to adsorption of VOCs, Pt_1/MnO_x (30 mg) is pretreated in 20 vol% O_2/He at 200 °C for 1 h. After being cooled down to 50 °C, the adsorption of VOCs is carried out under a flow of N_2 until adsorption saturation, as indicated by the stable signal of VOCs in the mass spectrometer. Then, a pure He flow is carried out for 20 min to clean the VOCs in the pipe. Finally, the VOCs desorption or oxidation is implemented followed by a flow of pure He (TPD) or 20%O_2/He (TPSR) by a step of 10 °C/min from 50 to 800 °C. The concentration of VOCs and the products (CO_2) are measured on-line by MS. The nomenclature list with all acronyms and parameters was summarized in Table S1.

2.3. Catalytic performance evaluation

Catalytic performance for the oxidation of toluene, *iso*-hexane, and their mixture are carried out in a continuous flow fixed-bed quartz tubular microreactor (i.d. = 6.0 mm). In order to avoid the hot spot, catalysts (0.05 g, 40–60 mesh) and quartz sand (0.25 g, 40–60 mesh) are well mixed. The reactant mixture includes 1000 ppm toluene or/and *iso*-hexane +40% O_2 + N_2 (balance). The 1000 ppm VOCs is obtained by passing a N_2 flow through two pure toluene- or *iso*-hexane—containing bottles that are chilled in an isothermal bath at 6 °C or −30 °C, respectively. The total flow of the reactant mixture is 33.4 mL/min, and the corresponding space velocity (SV) is 40,000 mL/(g h). Various

amount of water vapor is introduced by passing the reactant mixture through a water saturator at different temperature. Reactants and products are analyzed online by gas chromatography (GC—14 C, Shimadzu) with a flame ionization detector (FID), using a stabilwax—DA column (30 m in length) and a Carboxen 1000 column (3 m in length). VOCs conversion is defined as $(C_{inlet} - C_{outlet})/C_{inlet} \times 100\%$, where C_{inlet} and C_{outlet} are the inlet and outlet VOCs concentration in the feed stream, respectively. The catalytic performance over the present catalysts is tested under steady-state reaction conditions. The data are collected for three times after 20 min of each run at a given temperature.

The apparent activation energy (E_a) is calculated at VOCs oxidation conversions below 20%. E_a (kJ/mol) is estimated according to the Arrhenius equation: $k = A\exp(-E_a/RT)$, where k represents the rate constant (s^{-1}) and A is the pre-exponential factor, respectively. TOFs are calculated according to the equation: $TOFs = xC_0/(n_{Pt}\,D_{Pt})$, where x, C_0 (mol/s), n_{Pt} (mol), and D_{Pt} represent the conversion at a certain temperature, initial VOCs concentration per second, actual molar amount of Pt, and metal dispersions, respectively.

3. Results and discussion

3.1. Catalytic oxidation of toluene or iso-hexane

For furniture paints industry, toluene and *iso*-hexane are the most typical aromatic hydrocarbons and alkanes among the various VOCs. As shown in Fig. S1, we first investigate the catalytic activity of *x* wt% Pt_1/MnO_x catalysts (x = 0–0.56) for toluene oxidation. Apparently, 0.56 wt % Pt_1/MnO_x exhibits the best catalytic activity. The introduction of Pt species could effectively improve the catalytic activity for toluene oxidation, due to the rise in the noble metal loading (Lai et al., 2014; Kim et al., 2018). Considering the high loading of noble metal would limit the industrial application, the Pt_1/MnO_x catalyst with appropriate loading (0.16 wt%) is chosen for subsequent testing. From Fig. 1, we could find that H_2-Pt_1/MnO_x-200 shows slightly higher catalytic activity than Pt_1/MnO_x, with a temperature for 50% and 90% toluene conversion at 209 °C ($T_{50\%}$) and 219 °C ($T_{90\%}$), respectively. Compared with the MnO_x catalyst, the single-atom Pt catalysts greatly reduce the apparent activation energy (E_a) from 98−111 kJ/mol to 45–76 kJ/mol, and increase the turnover frequencies (TOFs) from 3.5−6.0 × 10^{-3} s^{-1} to 8.0−13.1 × 10^{-3} s^{-1} for toluene or *iso*-hexane oxidation (Table 1). Table S2 summarizes the catalytic activities of various catalysts for hexane oxidation. $T_{90\%}$ (237 °C) over H_2-Pt_1/MnO_x-200 (1000 ppm

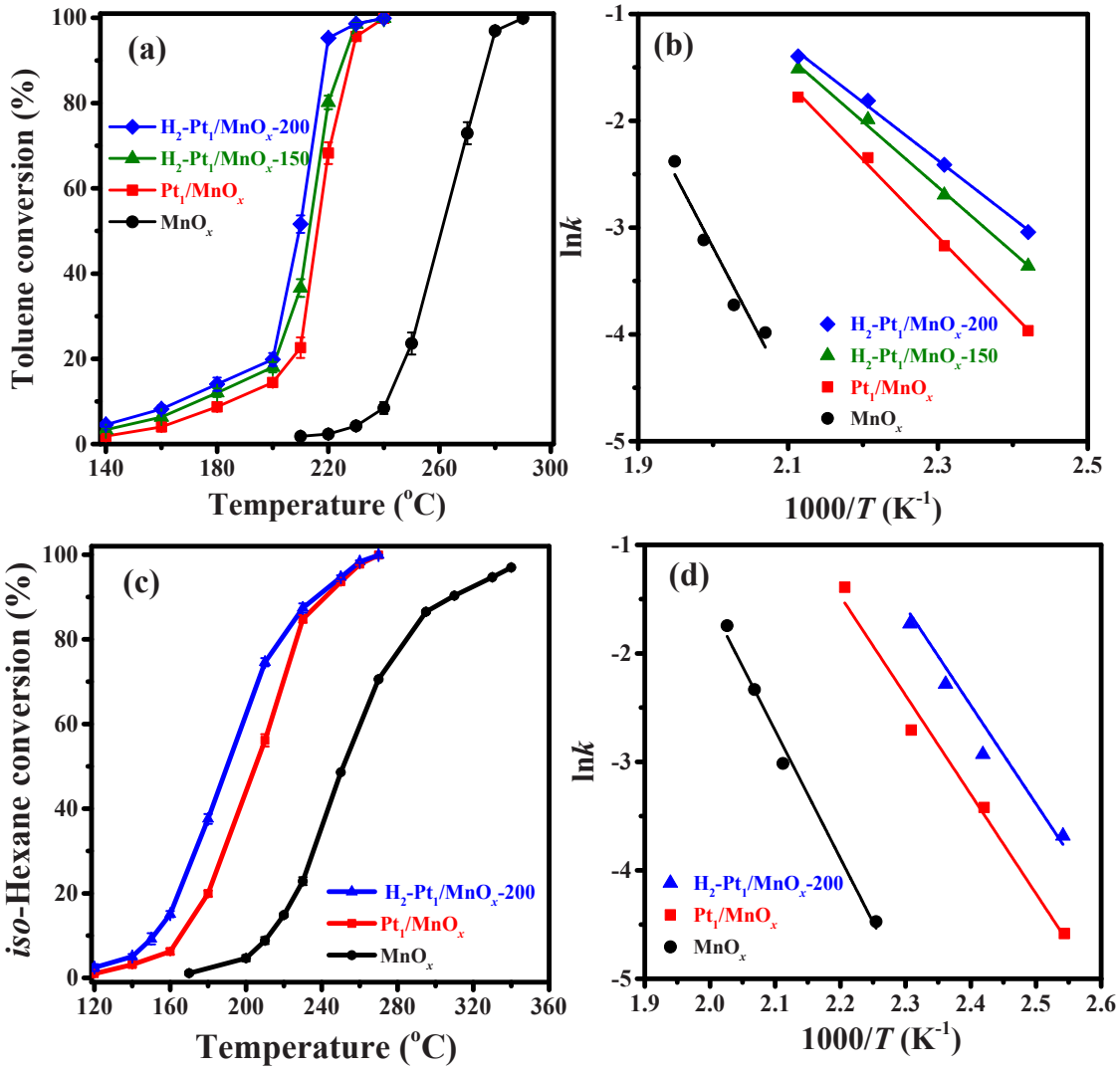

Fig. 1. (a) Toluene and (c) *iso*-Hexane conversion as a function of temperature as well as (b) Arrhenius plots for toluene and (d) *iso*-Hexane oxidation over the as-obtained samples at SV = 40,000 mL/(g h).

Table 1
Catalytic activities, TOFs, and apparent activation energies (E_a) of the samples at SV = 40,000 mL/(g h).

Samples	Toluene conversion		*iso*-Hexane conversion		TOF_{Pt} at 160 °C ($\times 10^{-3}$ s^{-1})		Metal dispersion[a] (%)	E_a[b] (kJ/mol)
	$T_{50\%}$ (°C)	$T_{90\%}$ (°C)	$T_{50\%}$ (°C)	$T_{90\%}$ (°C)	Toluene	*iso*-Hexane		
MnO_x	261	277	251	310	–	–	–	111/98
Pt_1/MnO_x	216	228	205	242	3.5	6.0	68	60/76
H_2-Pt_1/MnO_x-150	213	225	–	–	5.7	–	65	51/–
H_2-Pt_1/MnO_x-200	209	219	190	237	8.0	13.1	61	45/69

[a] Determined by the CO chemisorption.
[b] The data before and after "/" are measured for toluene oxidation and *iso*-hexane oxidation, respectively.

iso-hexane at SV = 40,000 mL/(g h)) is lower than that (ca. 260 °C) over 5% Pd(R)/Al_2O_3 (250 ppm *n*-hexane at SV = 108,000 mL/(g h)) (Ihm et al., 2004), and that (ca. 400 °C) over 0.1 wt% Pt/(stainless steel foil coated with a thin film of 7.1 wt% ZrO_2) (1500 ppm *n*-hexane at SV = 17,500 mL/(g h)) (Novaković et al., 2008), and that (ca. 475 °C) over $La_{0.75}Ag_{0.25}FeO_3$ (1500 ppm *n*-hexane at SV = 8900 mL/(g h)) (Kucharczyk et al., 2019), and that (ca. 290 °C) over 0.3 wt% Pt/hexagonal boron nitride (600 ppm *iso*-hexane at SV = 20,000 mL/(g h)) (Wu et al., 2001). In other words, the H_2-Pt_1/MnO_x-200 catalyst outperforms most of the above catalysts reported in literature.

The catalytic stability of the supported noble-metal catalyst is more important for industrial applications. As shown in Fig. 2a, the catalytic stability for toluene oxidation decreases in the order of H_2-Pt_1/MnO_x-200 > H_2-Pt_1/MnO_x-150 > Pt_1/MnO_x. The toluene conversion decreases sharply from 92% to 10% within 4 h over the Pt_1/MnO_x catalyst, while that over the MnO_x catalyst keeps stable. Only a negligible fluctuation is observed during the 16-h investigation over H_2-Pt/MnO_x-200. The reduction temperature, resulting in different reduction degree of the as-obtained samples, is shown to have an important influence on the catalytic stability. It is supposed that the stability of the catalyst with relative lower valence of platinum and manganese oxide could be greatly improved. Interestingly, the as-obtained samples exhibit good catalytic stability for *iso*-hexane oxidation, and *iso*-hexane conversion is not significantly changed within 16 h of steady-state oxidation (Fig. 2b).

3.2. Characterization of the as-obtained samples

A number of methods are carried out to investigate the key factors for the catalytic performance (especially catalytic stability). Fig. S2 shows the XRD patterns of the samples. It could be observed that the fresh samples dominantly display a cubic Mn_2O_3 (JCPDS PDF No. 41–1442) and tetragonal MnO_2 (JCPDS PDF No. 44–0141) structure, suggesting that the crystal structures of these manganese oxides are similar. Compared with the standard XRD patterns of tetragonal Mn_3O_4 (JCPDS PDF No.24–0734), two additional weak diffraction peaks at 32.32° and 36.08° appear in the H_2-Pt_1/MnO_x-200 sample, indicating that a part of manganese oxide is reduced during the H_2 treatment at a low temperature. After Pt doping, the intensities of diffraction peaks of the samples become broader and weaker. It is indicated that there is a strong interaction between platinum species and MnO_x. No diffraction peaks assignable to the Pt crystal phases are detected, due to the relatively high dispersion (61−68%, Table 1) and low loading of the noble metal.

To investigate the morphology and size of the as-obtained samples, SEM and HR—TEM are conducted. From the SEM images, it could be found that the MnO_x support exhibits a wire-like morphology with a mean diameter of 20–100 nm (Fig. S3a). TEM images display that the morphology of MnO_x after the introduction of Pt is not changed, while its average diameter becomes small (10–30 nm) (Fig. S3b). Atomic-resolution observation of the Pt atoms over H_2-Pt_1/MnO_x-200 is directly provided by the aberration-corrected HAADF—STEM result (Fig. 3). As clearly marked by the red circles, it can be seen that Pt atoms (bright spots) are atomically dispersed on the surface of MnO_x (dark substrate) without the presence of any Pt clusters/nanoparticles. Energy-dispersive spectroscopic (EDS) mappings further confirm that the Pt atoms are uniformly distributed on the supports. The in-situ DRIFTS of CO adsorption (Fig. S4) over MnO_x, Pt_1/MnO_x, and H_2-Pt_1/MnO_x-200 were detected after CO saturation and N_2 purging. The strong vibration bands at 2170 cm^{-1} and 2118 cm^{-1} could be due to the gas CO. The characteristic peak of single Pt atom usually appears at 2090 − 2115 cm^{-1}, but CO adsorption bands on $Pt^{\delta+}$ single-atom sites may also be observed in the low-frequency region (Zhang et al., 2017; Qiao et al., 2011; Xiao et al., 2021). The CO adsorption peak position and strength on the single atom sites are highly dependent on the catalysts. The shoulder peak at 2100 cm^{-1} and 2080 cm^{-1} over the

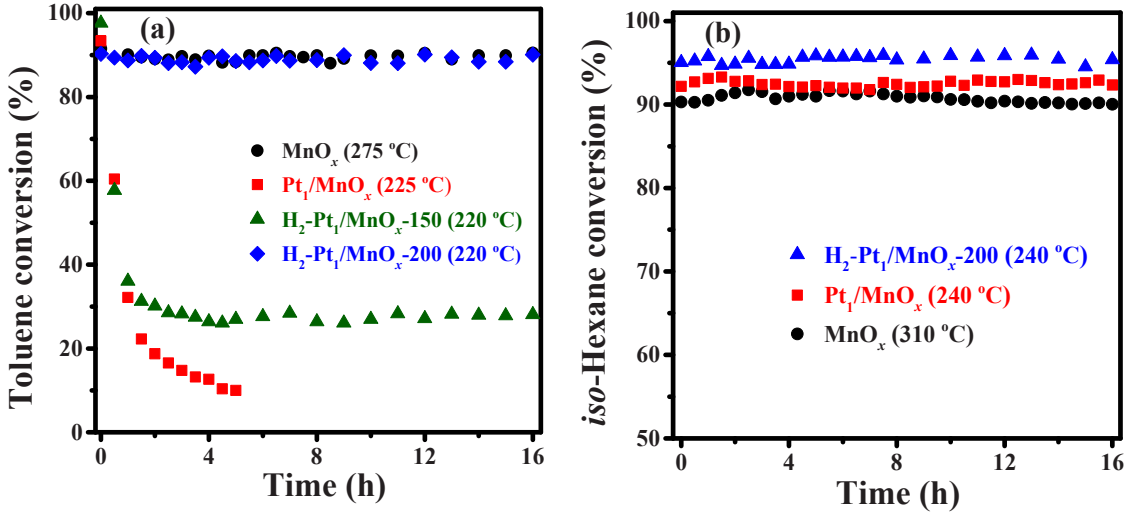

Fig. 2. (a) Toluene and (b) *iso*-hexane conversion over the as-obtained samples within 16 h of on-stream reaction.

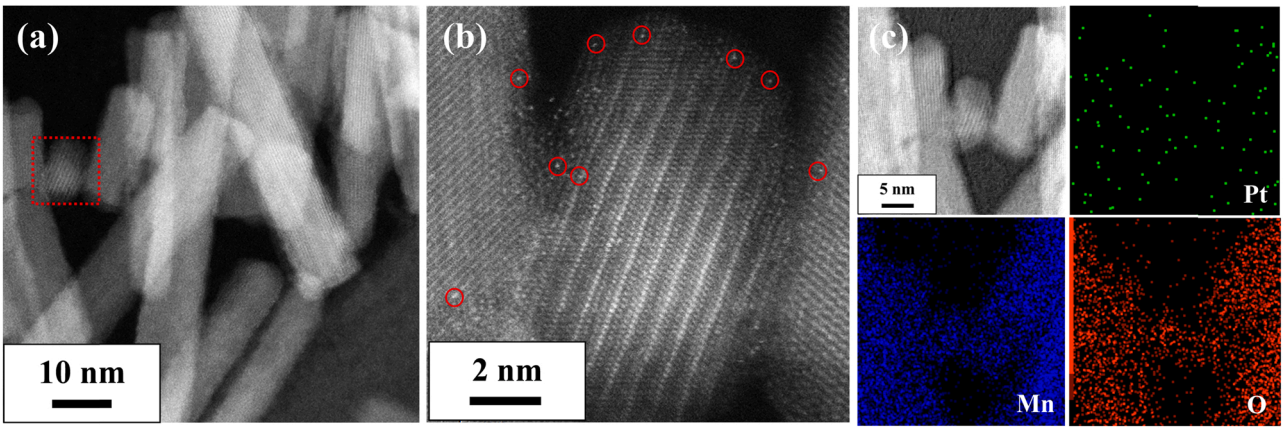

Fig. 3. (a) HAADF−STEM image, (b) partial enlarged HAADF−STEM image and (c) corresponding EDS elemental maps of the H_2-Pt_1/MnO_x-200 catalyst, showing the monoatomic separation of precious metals on the MnO_x carrier.

Pt_1/MnO_x and H_2-Pt_1/MnO_x-200 catalyst should be due to the CO adsorption bands on the $Pt^{\delta+}$ single-atom sites. Furthermore, it is weakly bound and easily desorbed after N_2 purging, suggesting that the weak interaction between adsorbed CO and $Pt^{\delta+}$ single-atom species. The signal at 1700–1900 cm^{-1} due to the bridge-bonded CO is not observed, indicating the absence of Pt clusters/nanoparticles. For the supported noble metal catalysts, in addition to the particle size of the noble metal, surface area also could affect the catalytic performance. The surface area of the Pt_1/MnO_x and H_2-Pt_1/MnO_x-200 catalyst is 72.4 and 74.2 m^2/g, respectively. Hence, we deduce that the great difference in the catalytic stability for the oxidation of toluene over the Pt_1/MnO_x and H_2-Pt_1/MnO_x-200 catalysts is not resulted from their small difference in the surface area.

Furthermore, XAFS measurement is used to further analyze the atomic structure of the as-obtained samples. X-ray absorption near-edge structure (XANES) spectra give the chemical state of platinum before and after H_2 treatment. As shown in Fig. 4a, the white-line peaks of the three samples are located between PtO_2 and $PtCl_2$ with shapes strongly resembling the curve of PtO_2, confirming that Pt species own the oxidation state between 2+ and 4+ valence states. The intensity of the white-line peak for the Pt_1/MnO_x sample is stronger than that for the reduced H_2-Pt_1/MnO_x-150 and H_2-Pt_1/MnO_x-200 samples, indicating that Pt atoms in Pt_1/MnO_x are more positively charged (Qiao et al., 2011; Xu et al., 2020). In other words, the valence state of Pt decreases with an increase in the reduction temperature. Extended X-ray absorption fine structure (EXAFS) spectra of the as-obtained samples and the reference samples are shown in Figs. 4b and S5, and the fitting results are given in Table S3. The spectra of the Pt_1/MnO_x, H_2-Pt_1/MnO_x-150 and H_2-Pt_1/MnO_x-200 samples exhibit a nearly identical shape, with a slight shift of the first nearest coordination peaks in the R space, compared to that of platinum oxide (only oxygen nearest neighbors). The similarity in the spectra indicates that the coordination environment is not significantly changed before and after reduction (Liu et al., 2018). The spectroscopy of the as-obtained samples show a prominent Pt−O bond distance of 2.00, 2.03 and 2.04 Å (PtO_2: 2.02 Å), while the peak of the Pt−Pt shell contribution at 2.76 Å is absent, further confirming the isolated Pt atoms are bonded to MnO_x via the Pt−O bonds (Wang et al., 2020a). Combined with the results of STEM, the H_2-Pt_1/MnO_x-150 and H_2-Pt_1/MnO_x-200 samples contain single-atom Pt species, which are well anchored on the surface of MnO_x during the reduction process. In addition, the Pt–O bond distance of the samples similar to that in PtO_2 suggests the existence of strong metal–support interaction (Chen et al., 2019). The main difference between fresh Pt_1/MnO_x and reduced samples is the coordination number, with 4.0 for H_2-Pt_1/MnO_x-150, 3.1 for H_2-Pt_1/MnO_x-200, and 6.0 for Pt_1/MnO_x. It is indicated that each Pt atom coordinated with fewer oxygen atoms on the support after reduction treatment. The different catalytic stability for toluene oxidation is likely related to the different local coordination

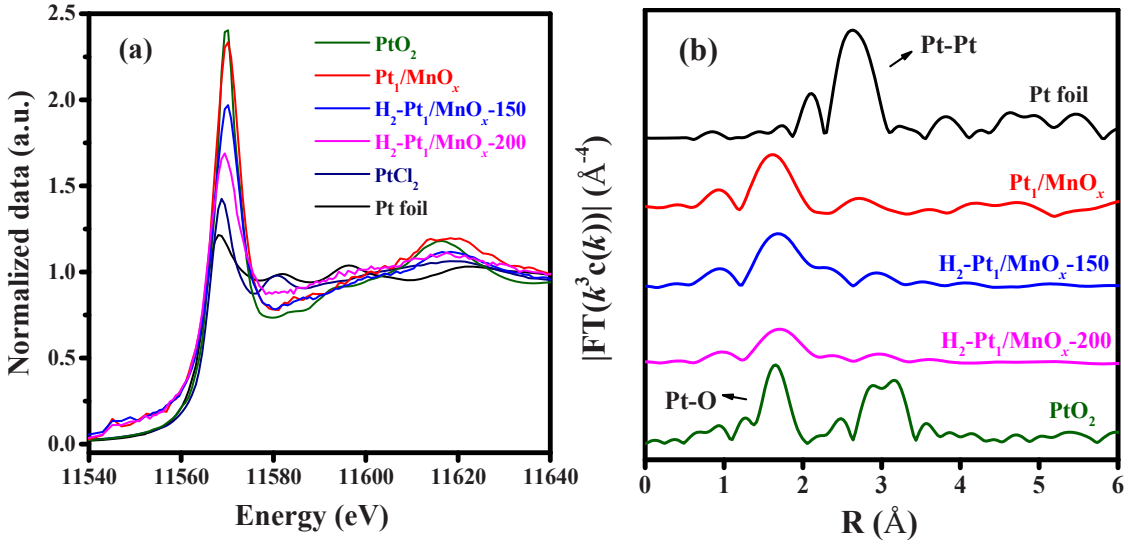

Fig. 4. (a) Pt L_3-edge XANES spectra and (b) Fourier transforms of EXAFS at the Pt L_3-edge spectra of the as-obtained samples.

environments near the single-atom Pt in the samples.

Redox properties of the as-obtained samples are evaluated using the H_2-TPR technique, and their profiles are shown in Fig. 5a. The main reduction peaks of MnO_x are at 334, 431, and 572 °C, which are attributed to the reduction of MnO_2 to Mn_2O_3, Mn_2O_3 to Mn_3O_4, and Mn_3O_4 to MnO, respectively (Chen et al., 2021; Yang et al., 2019b). The reduction peaks at 242 °C over Pt_1/MnO_x, and at 128 °C over H_2-Pt_1/MnO_x-200 are assigned to the reduction of manganese oxide and PtO_x. The reduction peak of the Pt_1/MnO_x sample significantly shifts to lower temperature compared with that of the MnO_x sample, indicating that introduction of Pt_1 atoms into transition-metal oxides significantly improves the reduction of MnO_x via the hydrogen spillover (Abbasi et al., 2011; Wu et al., 2017). The reduction peak of the H_2-Pt_1/MnO_x-200 sample shifts to the lowest temperature (128 °C), revealing that hydrogen reduction treatment of the fresh Pt_1/MnO_x sample could effectively weaken the Mn−O bond and improve oxygen species mobility (Liu et al., 2019).

O_2-TPD measurements are carried out to further evaluate the oxygen mobility of the samples (Fig. 5b). Generally, the desorption of lattice oxygen occurs at higher temperature (> 300 °C) and the peak shape is not symmetric (Li et al., 2011). The peaks at 339 °C and 405 °C could be assigned to the desorption of surface lattice oxygen, due to the existence of interaction between Pt and MnO_x species. The other peaks in the range of 400−800 °C could be assigned to the desorption of bulk lattice oxygen (Si et al., 2015; Yang et al., 2019a). For H_2-Pt_1/MnO_x-200, it should be mentioned that the initial desorption peaks shift to a lower temperature, which further indicates an enhancement in surface lattice oxygen mobility (Liotta et al., 2013; Hua et al., 2019). The surface Mn—O bonds could be more facilely broken and oxygen species migration from sub-surface to surface are accelerated over the reduced samples (Si et al., 2015), which is in consistency with the results of H_2—TPR. In addition, the desorption peak intensity of H_2-Pt_1/MnO_x-200 decreases compared with that of Pt_1/MnO_x, indicating the reduced sample contains more low-valence manganese oxide after the hydrogen treatment.

XPS is carried out to investigate the possible role of oxygen in VOCs oxidation reaction. The O 1s XPS spectra (Fig. 5c and d) could be decomposed into three components, lattice oxygen (O^{2-}_{latt}) at 529.5−529.6 eV, adsorbed oxygen (O_{ads}, including O^-, O_2^-, and O_2^{2-}) at 531.3 eV, and adsorbed molecular water species at 533.4 eV (Deng et al., 2015). We find that the relative amount of surface $O^{2-}_{latt}/(O_{ads} + O^{2-}_{latt})$ molar ratios in the fresh and used Pt_1/MnO_x samples keep stable, while that in the fresh and used H_2-Pt_1/MnO_x-200 samples increase from 0.71 to 0.81. More information on the oxygen vacancy could be obtained

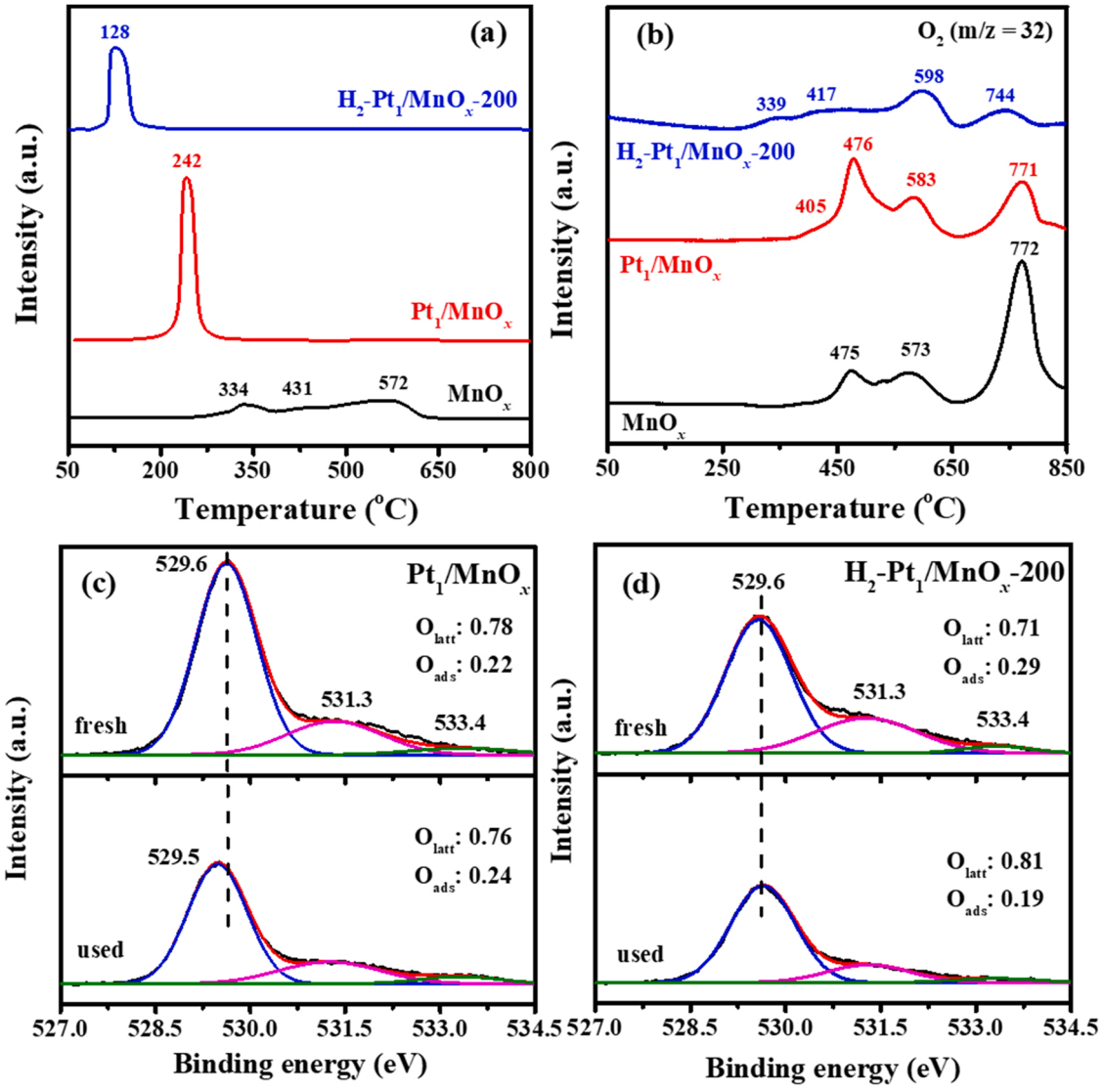

Fig. 5. (a) H_2-TPR and O_2-TPD profiles of MnO_x, Pt_1/MnO_x, and H_2-Pt_1/MnO_x-200; (c) and (d) O 1s XPS spectra of the fresh and used Pt_1/MnO_x, and H_2-Pt_1/MnO_x-200 catalyst.

via the Raman technique (Fig. S6). The bands at 345 or 351, 565 or 581, and 638 or 644 cm^{-1} over Pt_1/MnO_x and H_2-Pt_1/MnO_x-200, are ascribed to the bending modes, asymmetric stretch of Mn–O–Mn, and symmetric stretch of Mn_2O_3/Mn_3O_4 groups, respectively. The band at 638 cm^{-1} over Pt_1/MnO_x shifts to 644 cm^{-1} over H_2-Pt_1/MnO_x-200, indicating that there are more oxygen vacancy defects in H_2-Pt_1/MnO_x-200 (Han et al., 2006; Zheng et al., 2021). The generation of surface O_{ads} (i.e., change O_2 to O^-, O_2^-, and O_2^{2-}) species involves the adsorption of O_2 on the surface oxygen vacancy, and the dissociation of the adsorbed O_2 species, accompanied with the oxidation of low valent Mn and Pt species (Yang et al., 2021). The surface O^{2-}_{latt} species are consumed due to the oxidation of adsorbed VOCs molecules, meanwhile the high valent Mn and Pt species, bonded with the surface O^{2-}_{latt} species, are reduced to low valent ions in order to maintain electrical neutrality. In addition, the replenishment of surface O^{2-}_{latt} species from the surface O_{ads} (O^-, O_2^-, and O_2^{2-}) species is also associated with the oxidation of low valent Mn and Pt species. Obviously, the surface O_{ads} species and the redox ability of the Pt_1/MnO_x and H_2-Pt_1/MnO_x-200 samples have a great influence on the supplement of surface O^{2-}_{latt} species. From the results of XPS and H_2-TPR characterization, we find that H_2-Pt_1/MnO_x-200 exhibits larger surface O_{ads} species and better low temperature reducibility than Pt_1/MnO_x. Therefore, the timely supplement of surface O^{2-}_{latt} species is understandable in the H_2-Pt_1/MnO_x-200 catalyst.

3.3. Possible influence factors on catalytic stability for VOCs oxidation

In order to investigate the possible reason for the quick deactivation of Pt_1/MnO_x, the used catalyst after evaluation for toluene removal is further characterized via the XRD and FTIR technique (Fig. S7A). It can be seen that the crystal structure of the deactivated Pt_1/MnO_x catalyst is not changed, compared with the fresh counterpart, which is understandable due to the adopted reaction temperature below than the calcination temperature of 380 °C. As shown in the FTIR spectra (Fig. S7B), the characteristic signals due to MnO_2 and Mn_2O_3 are observed at 2940 cm^{-1}, 1386 cm^{-1}, 730 cm^{-1}, 527 cm^{-1}, and 460 cm^{-1}, and that due to the frequency modes of the –OH group are observed at 3445 cm^{-1}, 1638 cm^{-1}, and 1115 cm^{-1} (Amsaveni et al., 2020; Venkateswarlu et al., 2020). It should be pointed out that the signals due to the deposition of carbon species are not detected. Hence, the quick deactivation of Pt_1/MnO_x might not be associated with the crystal structure and the carbon deposition. Combined with the catalytic performance and characterization results, the difference in the catalytic stability of Pt_1/MnO_x and H_2-Pt_1/MnO_x-200 for toluene oxidation could be roughly ascribed to the different surface properties of platinum and manganese oxide.

The adsorption ability for toluene over the as-obtained catalysts is evaluated by toluene—TPD (Fig. 6a). The intensity of desorption peak shows the desorption capacity for toluene in the catalysts, while the temperature of desorption peak indicates the interaction between toluene and catalyst. Both Pt_1/MnO_x and H_2-Pt_1/MnO_x-200 exhibit better toluene adsorption capacity than MnO_x. Compared with H_2-Pt_1/MnO_x-200, the desorption peak of Pt_1/MnO_x is detected at a relatively higher temperature, and the total desorption amount of toluene increases, indicating that the interaction between toluene and Pt_1/MnO_x is much stronger than that of H_2-Pt_1/MnO_x-200 (Gan et al., 2019). Toluene desorption amount significantly increases after Pt loading, indicating that noble metal Pt is the main adsorption site for toluene. It should be noted that although the high coverage of reactants is essential factor for enhancing catalytic reaction, too much adsorption of toluene on the Pt single atoms might not be favorable for the long term catalytic stability of Pt_1/MnO_x. Combined with the context above, the Pt coordination structural might be related with the ability for toluene adsorption, and the Pt single atoms coordinated more oxygen atoms benefit toluene adsorption. Previous studies (Thang et al., 2018; Li et al., 2021) show that the Pt coordination number has a direct influence on the reactant adsorption over the supported single atom Pt catalysts. In case of Pt_1-Fe_2O_3, after the heat treatment in air, Pt atoms are oxidized into higher valence state, which can effectively promote the adsorption capacity to ethanol. In the present study, a simple hydrogen reduction treatment of Pt_1/MnO_x greatly weakens (one tenth) the adsorption ability for toluene (Fig. 6a), due to decrease in the valence state of Pt. However, the real reasons need further investigation. A small difference in the *iso*-hexane adsorption (Fig. S8) is observed over the Pt_1/MnO_x and H_2-Pt_1/MnO_x-200 samples. In other words, the nature of the reactant also has an important influence on its adsorption over the supported single atom catalyst.

TPSR profiles of toluene oxidation over Pt_1/MnO_x and H_2-Pt_1/MnO_x-200 are also measured (Fig. 6b). The CO_2 signals recorded below 400 °C could be ascribed to the CO_{2I} (type I, in green area), originated from the reaction between surface O^{2-}_{latt} species and toluene, and these recorded above 400 °C could be ascribed to CO_{2II} (type II, in blue area), originated from the reaction between inactive bulk O^{2-}_{latt} and toluene. For Pt_1/MnO_x, the adsorbed toluene hard reacts with surface O^{2-}_{latt} species, resulting in the temperature for the generation of CO_{2I} increases than that for H_2-Pt_1/MnO_x-200. Because the inactive bulk O^{2-}_{latt} might

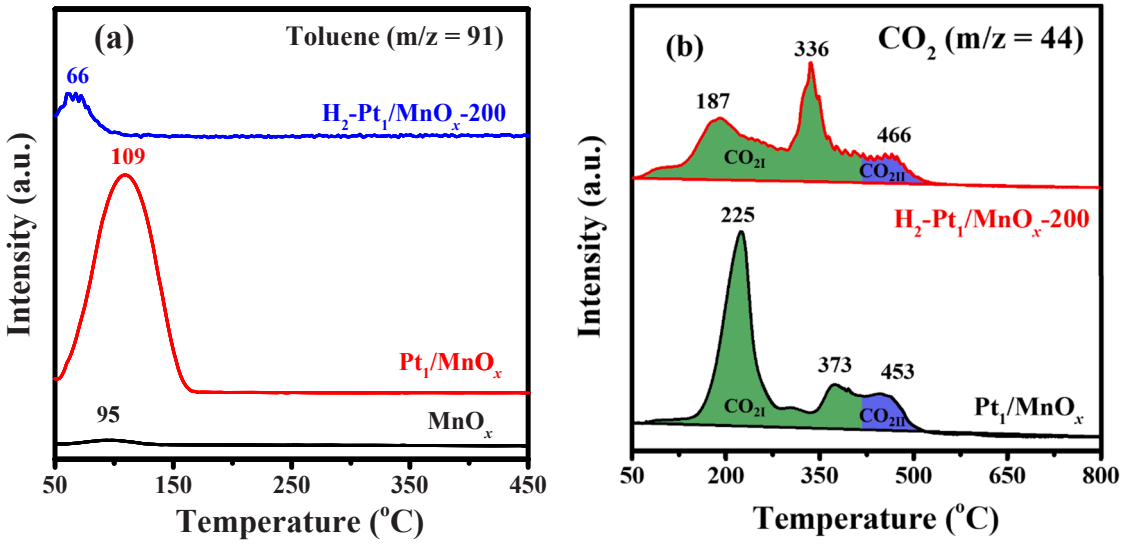

Fig. 6. Toluene−TPD and Toluene−TPSR profiles of as-obtained samples.

hardly participate in reaction, a little amount of CO_{2II} is detected over Pt_1/MnO_x and H_2-Pt_1/MnO_x-200 at a similar temperature. According to the above results, H_2-Pt_1/MnO_x-200 with weak Mn—O bonds shows better catalytic activity and stability, due to the high reactivity and the quick replenishment of the surface $O^{2-}{}_{latt}$ species. Hence, it is suggested that the lattice oxygen mobility of the support might be another important factor for catalytic stability.

Under the present reaction conditions, the complete oxidation of VOCs over Pt_1/MnO_x and H_2-Pt_1/MnO_x-200 follows the Mars–van Krevelen mechanism. In other words, the oxidation reaction occurs between the adsorbed VOCs molecules on Pt_1 atoms and the surface $O^{2-}{}_{latt}$ species of manganese oxide. Therefore, both the $O^{2-}{}_{latt}$ mobility and VOCs adsorption play an important role in the catalytic performance. To ensure the continuous oxidation of toluene, the consumed surface $O^{2-}{}_{latt}$ should be regenerated by the activation of O_2 accompanied with the recycle of Mn^{3+}−Mn^{4+} (Luo et al., 2019). In the case of H_2-Pt_1/MnO_x-200, reduction treatment decreases the Pt—O coordination number and the strength of Mn−O bonds. As mentioned above, noble metal Pt is the main adsorption site for toluene, and the lower Pt—O coordination number could lead to weaker toluene adsorption ability. According to the results of XPS and H_2-TPR characterization, H_2-Pt_1/MnO_x-200 exhibits larger surface O_{ads} species and better low temperature reducibility than Pt_1/MnO_x, and the timely supplement of surface $O^{2-}{}_{latt}$ species could be well proceeded in the H_2-Pt_1/MnO_x-200 catalyst. As shown in Fig. 2a, toluene conversion is not changed during 16 h of on-stream reaction over the H_2-Pt_1/MnO_x-200 sample, because the consumed surface $O^{2-}{}_{latt}$ species, which reacted with the proper adsorbed toluene, could be timely supplied. On the other hand, too much adsorption of toluene on Pt_1/MnO_x could not be totally oxidized due to the lack of surface $O^{2-}{}_{latt}$ species. The supplement of surface $O^{2-}{}_{latt}$ species is related with the surface O_{ads} species and the redox ability of catalyst. If the consumed surface $O^{2-}{}_{latt}$ species could not be timely supplied, the adsorbed toluene molecules could not be completely oxidized into CO_2 and H_2O. The unreacted adsorbed toluene molecules, and the partial oxidation intermediates will cover the reactive sites, and then decrease the reaction rate. As illustrated in Fig. 7, the synergistic effect between toluene adsorption and lattice oxygen mobility is the key factor of the catalytic stability for toluene oxidation. In order to enhance the catalytic stability for toluene oxidation, it is necessary to properly reduce the adsorption ability for toluene, and improve the supplement of surface $O^{2-}{}_{latt}$ species. Interestingly, such a goal could be achieved via the simple hydrogen reduction treatment of Pt_1/MnO_x.

Both Pt_1/MnO_x and H_2-Pt_1/MnO_x-200 show good catalytic stability for *iso*-hexane oxidation. In addition to the intrinsic physicochemical properties of the VOCs, the adsorption behavior of the VOCs over the catalyst can greatly influence the catalytic stability. As shown in Fig. S9, it could be seen that over the Pt_1/MnO_x sample, *iso*-hexane desorption takes place at a lower temperature. Toluene-TPD and *iso*-hexane-TPD results clearly suggest that adsorption ability of Pt_1/MnO_x for alkane is much weaker than that for aromatic hydrocarbon, and much more toluene molecules could be adsorbed over Pt_1/MnO_x than *iso*-hexane molecules under the same conditions. The methyl group in the toluene molecules increases the electronic density of the aromatic ring, and the Pt_1 atom is easy to accept the π electrons provided by the aromatic ring (J. Zhang, 2018; Y.H. Zhang, 2018). Many researches have reported the different adsorption behavior of various VOCs over the same catalyst (Mazzarino and Barresi, 1993; Ordóñez et al., 2002). In the present study, *iso*-hexane and toluene show very different adsorption behavior over the Pt_1/MnO_x catalyst, and the CO_2 generation is mainly depended on the nature of surface $O^{2-}{}_{latt}$ species.

3.4. Catalytic performance for the complete oxidation of VOCs mixture

Usually, industrial emissions contain various VOCs. Hence, we also investigate the catalytic activity of H_2-Pt_1/MnO_x-200 for the complete oxidation of 1000 ppm (toluene + *iso*-hexane) mixture. It is well known that the mixture effect in the multicomponent VOCs oxidation is due to the different adsorption and activation property of the various VOCs over the catalyst. As shown in Fig. 8 and Table S4, with the same concentration, the presence of toluene significantly inhibits the catalytic oxidation of *iso*-hexane, while the presence of *iso*-hexane has minor effect on toluene oxidation. When the total concentration of VOCs mixture keeps constant in feeding streams, the catalytic activity of H_2-Pt_1/MnO_x-200 for toluene oxidation is enhanced with a decrease in the toluene concentration, while that for *iso*-hexane oxidation is enhanced with an increase in the *iso*-hexane concentration. Such a result is associated with the competitive adsorption of toluene and *iso*-hexane, and the much stronger adsorption of the aromatic compounds on the noble metal surface (Zhao et al., 2020). The catalytic stability of H_2-Pt_1/MnO_x-200 for the oxidation of (500 ppm toluene + 500 ppm *iso*-hexane) mixture is shown in Fig. S10. It could be found that the VOCs conversion exhibits a steady state within 10-h on-stream reaction time. In other words, H_2-Pt_1/MnO_x-200 is stable for the complete oxidation of VOCs mixture.

3.5. Effect of relative humidity on catalytic performance

For practical application, water is commonly found in industrial exhaust streams, and it is important to develop a catalyst with high resistance to water. Therefore, we investigate the catalytic activity of

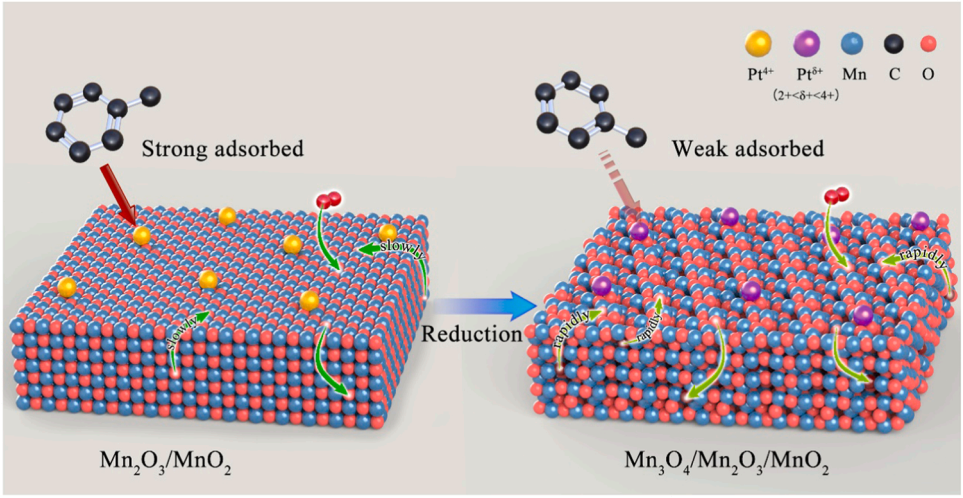

Fig. 7. Schematic illustration of catalytic stability for toluene removal over the Pt_1/MnO_x and H_2-Pt_1/MnO_x-200 catalyst.

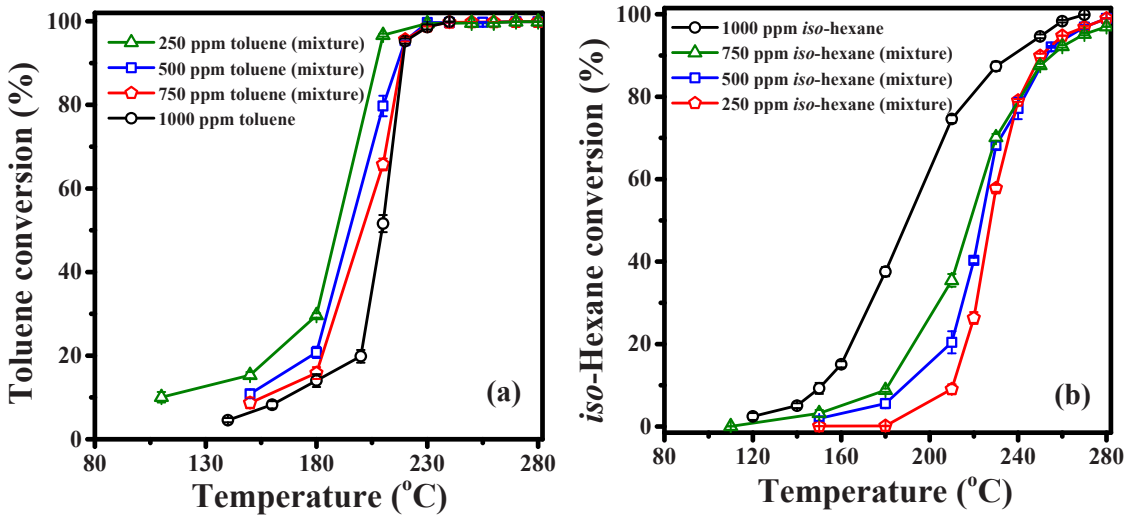

Fig. 8. Conversion of toluene and *iso*-hexane separately and in the mixture over H_2-Pt_1/MnO_x-200 as a function of reaction temperature under the reaction conditions of (toluene + *iso*-hexane) concentration = 1000 ppm, (toluene + *iso*-hexane)/O_2 molar ratio = 1/400, and SV = 40,000 mL/(g h).

H_2-Pt_1/MnO_x-200 for the oxidation of (500 ppm toluene +500 ppm *iso*-hexane) in the presence of different amount of water vapor. Compared with the VOCs conversion under dry reaction condition, the conversion at relative humidity (RH) = 25% slightly increases, as shown in Fig. 9. The presence of little water vapor has a positive effect on VOCs removal due to the formation of hydroperoxyl species (Zhao et al., 2020). Similar phenomenon was also observed over the supported AuPd and Pt nanocatalysts for toluene and benzene oxidation (Xie et al., 2015; Yang et al., 2019a). The generation of hydroperoxyl species through H-transfer reaction ($O_2^* + H_2O^* \rightarrow OOH^* + OH^*$ and $OOH^* \rightarrow O^* + OH^*$) could easily activate the adsorbed O_2 molecules on the noble metal sites in the presence of H_2O. However, a slight deactivation is observed in terms of $T_{50\%}$ and $T_{90\%}$, with a rise in the RH from 25% to 100%. The inhibitory effect on VOCs removal in the presence of a larger amount of water vapor could be attributed to the competitive adsorption of water and O_2 molecules on the catalyst surface (Li et al., 2020; Bhat et al., 2021). Shown in Fig. S11 is the catalytic stability of H_2-Pt_1/MnO_x-200 at 200, 230, or 240 °C with various relative humidity. Negligible change in VOCs conversion could be observed, indicating H_2-Pt_1/MnO_x-200 is stable even in the presence of water vapor for the complete oxidation of VOCs mixture.

4. Conclusions

In summary, MnO_x nanowires supported Pt single-atom catalyst (Pt_1/MnO_x) is obtained via the molten salt method. The presence of Pt single atom promotes the catalytic activity for the oxidation of toluene and *iso*-hexane. The catalytic stability of Pt_1/MnO_x for toluene oxidation is dominated by a balance between toluene adsorption and lattice oxygen mobility. A proper H_2 reduction treatment of Pt_1/MnO_x at 200 °C (H_2-Pt_1/MnO_x-200) benefits the generation of Pt–O with low coordination number and the weak Mn–O bonds, resulting in the decreased adsorption of toluene and enhanced mobility of lattice oxygen. A facile redox ability of H_2-Pt_1/MnO_x-200 contributes the reversible cycles of lattice oxygen, the consumed surface O^{2-}_{latt} species could be quickly replenished, and then the catalytic stability is greatly improved. Although the presence of toluene significantly inhibits the catalytic oxidation of *iso*-hexane, H_2-Pt_1/MnO_x-200 exhibits good catalytic stability for the oxidation of (toluene + *iso*-hexane) mixture with or without the presence of water vapor. The present study indicates that the H_2 reduction treatment is an interesting method for the enhancement of supported noble metal single-atom catalyst for VOCs removal.

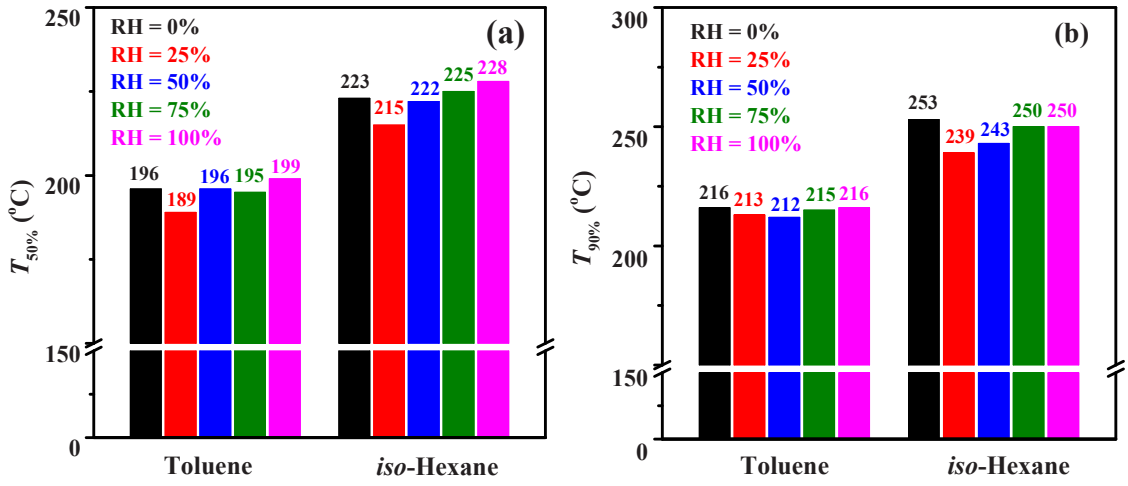

Fig. 9. Effects of relative humidity (RH) on (a) $T_{50\%}$ and (b) $T_{90\%}$ over H_2-Pt_1/MnO_x-200 as a function of reaction temperature under the reaction conditions of 500 ppm toluene and 500 ppm *iso*-hexane, (toluene + *iso*-hexane)/O_2 molar ratio = 1/400, and SV = 40,000 mL/(g h).

CRediT authorship contribution statement

Yuan Feng: Carried out experiments, Wrote and modified the manuscript. **Chongchen Wang, Can Wang, Haibao Huang, Hsing-Cheng His, Erhong Duan Yuxi Liu, Guangsheng Guo and Hongxing Dai:** Analyzed the experimental results. **Jiguang Deng:** Designed the experiments, Analyzed the experimental results, Wrote and modified the manuscript.

Declaration of Competing Interest

The authors declare that they have no known competing financial interests or personal relationships that could have appeared to influence the work reported in this paper.

Acknowledgments

This work was supported by the Natural Science Foundation of China (21961160743, 21622701, U1507108, and 21477005), National Key R&D Program of China (2016YFC0204800) and Natural Science Foundation of Hebei Province-Key Project (B2021208033).

Appendix A. Supporting information

Supplementary data associated with this article can be found in the online version at doi:10.1016/j.jhazmat.2021.127337.

References

Abbasi, Z., Haghighi, M., Fatehifar, E., Saedy, S., 2011. Synthesis and physicochemical characterizations of nanostructured Pt/Al_2O_3–CeO_2 catalysts for total oxidation of VOCs. J. Hazard. Mater. 186, 1445–1454.

Amsaveni, P., Nivetha, A., Sakthivel, C., Philip, C.S., Prabha, I., 2020. Effectiveness of surfactants for unique hierarchical Mn_2O_3 nanomaterials as enhanced oxidative catalysts, antibacterial agents, and photocatalysts. J. Phys. Chem. Solids 144, 109429.

Bhat, A., Hill, A.J., Fisher, G.B., Schwank, J.W., 2021. Improving the thermal stability and *n*-butanol oxidation activity of Ag-TiO_2 catalysts by controlling the catalyst architecture and reaction conditions. Appl. Catal. B: Environ. 297, 120476.

Cao, R.R., Zhang, P.Y., Liu, Y., Zheng, X.M., 2019. Ammonium-treated birnessite-type MnO_2 to increase oxygen vacancies and surface acidity for stably decomposing ozone in humid condition. Appl. Surf. Sci. 495, 143607.

Chen, W.L., Ma, Y.L., Li, F., Pan, L., Gao, W.P., Xiang, Q., Shang, W., Song, C.Y., Tao, P., Zhu, H., Pan, X.Q., Deng, T., Wu, J.B., 2019. Strong electronic interaction of amorphous Fe_2O_3 nanosheets with single-atom Pt toward enhanced carbon monoxide oxidation. Adv. Funct. Mater. 29, 1904278.

Chen, L.Z., Liu, Y.J., Fang, X., Cheng, Y., 2021. Simple strategy for the construction of oxygen vacancies on α-MnO_2 catalyst to improve toluene catalytic oxidation. J. Hazard. Mater. 409, 125020.

Deng, J.G., He, S.N., Xie, S.H., Yang, H.G., Liu, Y.X., Guo, G.S., Dai, H.X., 2015. Ultralow loading of silver nanoparticles on Mn_2O_3 nanowires derived with molten salts: a high-efficiency catalyst for the oxidative removal of toluene. Environ. Sci. Technol. 49, 11089–11095.

Feng, X.S., Luo, F.Q., Chen, Y.Y., Lin, D.F., Luo, Y.J., Xiao, L.R., Liu, X.P., Sun, X.L., Qian, Q.R., Chen, Q.H., 2021. Boosting total oxidation of propane over CeO_2@Co_3O_4 nanofiber catalysts prepared by multifluidic coaxial electrospinning with continuous grain boundary and fast lattice oxygen mobility. J. Hazard. Mater. 406, 124695.

Gan, T., Chu, X.F., Qi, H., Zhang, W.X., Zou, Y.C., Yan, W.F., Liu, G., 2019. Pt/Al_2O_3 with ultralow Pt-loading catalyze toluene oxidation: promotional synergistic effect of Pt nanoparticles and Al_2O_3 support. Appl. Catal. B: Environ. 257, 117943.

Gao, X.M., Gao, K.L., Zhu, W., Liang, C.H., Li, Q.E., Fu, F., Zhu, Y.F., 2021. Accurate guided alternating atomic layer enhance internal electric field to steering photogenerated charge separation for enhance photocatalytic activity. Appl. Catal. B: Environ. 298, 120536.

Han, Y.F., Chen, F.X., Zhong, Z.Y., Ramesh, K., Widjaja, E., Chen, L.W., 2006. Synthesis and characterization of Mn_3O_4 and Mn_2O_3 nanocrystals on SBA-15: novel combustion catalysts at low reaction temperatures. Catal. Commun. 7, 739–744.

Hua, W.C., Zhang, C.H., Guo, Y.L., Chai, G.T., Wang, C., Guo, Y., Wang, L., Wang, Y.S., Zhan, W.C., 2019. An efficient $Sn_yMn_{1-y}O_x$ composite oxide catalyst for catalytic combustion of vinyl chloride emissions. Appl. Catal. B: Environ. 255, 117748.

Ihm, S.K., Jun, Y.D., Kim, D.C., Jeong, K.E., 2004. Low-temperature deactivation and oxidation state of Pd/γ-Al_2O_3 catalysts for total oxidation of *n*-hexane. Catal. Today 93–95, 149–154.

Kim, J.M., Kim, J.H., Lee, C.Y., Jerng, D.W., Ahn, H.S., 2018. Toluene and acetaldehyde removal from air on to graphene-based adsorbents with microsized pores. J. Hazard. Mater. 344, 458–465.

Kucharczyk, B., Adamska, K., Tylus, W., Miśta, W., Szczygieł, B., Winiarski, J., 2019. Effect of silver addition to $LaFeO_3$ perovskite on the activity of monolithic $La_{1-x}Ag_xFeO_3$ perovskite catalysts in methane hexane oxidation. Catal. Lett. 149, 1919–1933.

Lai, T.Y., Chen, T.C., Lan, Y.K., Chen, B.S., You, J.H., Yang, C.M., Lai, N.C., Wu, J.H., Chen, C.S., 2014. Pt/SBA-15 as a highly efficient catalyst for catalytic toluene oxidation. ACS Catal. 4, 3824–3836.

Li, P., He, C., Cheng, J., Ma, C.Y., Dou, B.J., Hao, Z.P., 2011. Catalytic oxidation of toluene over Pd/Co_3AlO catalysts derived from hydrotalcite-like compounds: Effects of preparation methods. Appl. Catal. B: Environ. 101, 570–579.

Li, Q.H., Li, Z., Zhang, Q.H., Zheng, L.R., Yan, W.S., Liang, X., Gu, L., Chen, C., Wang, D. S., Peng, Q., Li, Y.D., 2021. Porous γ-Fe_2O_3 nanoparticle decorated with atomically dispersed platinum: study on atomic site structural change and gas sensor activity evolution. Nano Res. 14, 1435–1442.

Li, Q.Q., Su, G.J., Li, C.Q., Wang, M.J., Tan, L., Gao, L.R., Mingge, W., Wang, Q.L., 2019. Emission profiles, ozone formation potential and health-risk assessment of volatile organic compounds in rubber footwear industries in China. J. Hazard. Mater. 375, 52–60.

Li, Z., Yan, Q.H., Jiang, Q., Gao, Y.S., Xue, T.S., Li, R.N., Liu, Y.F., Wang, Q., 2020. Oxygen vacancy mediated $Cu_yCo_{3-y}Fe_1O_x$ mixed oxide as highly active and stable toluene oxidation catalyst by multiple phase interfaces formation and metal doping effect. Appl. Catal. B: Environ. 269, 118827.

Liotta, L.F., Wu, H.J., Pantaleo, G., Venezia, A.M., 2013. Co_3O_4 nanocrystals and Co_3O_4-MO_x binary oxides for CO, CH_4 and VOC oxidation at low temperatures: a review. Catal. Sci. Technol. 3, 3085–3102.

Liu, L.Z., Li, J.X., Zhang, H.B., Li, L., Zhou, P., Meng, X.L., Guo, M.M., Jia, J.P., Sun, T.H., 2019. In situ fabrication of highly active γ-MnO_2/$SmMnO_3$ catalyst for deep catalytic oxidation of gaseous benzene, ethylbenzene, toluene, and o-xylene. J. Hazard. Mater. 362, 178–186.

Liu, R., Chen, H.M., Fang, L.P., Xu, C.H., He, Z.L., Lai, Y.J., Zhao, H.C., Bekana, D., Liu, J. F., 2018. Au@Pd bimetallic nanocatalyst for carbon−halogen bond cleavage: an old story with new insight into how the activity of Pd is Influenced by Au. Environ. Sci. Technol. 52, 4244–4255.

Luo, M.M., Cheng, Y.X., Peng, Z., Pan, W., 2019. Copper modified manganese oxide with tunnel structure as efficient catalyst for low-temperature catalytic combustion of toluene. Chem. Eng. J. 369, 758–765.

Ma, M.D., Yang, R., He, C., Jiang, Z.Y., Shi, J.W., Albilali, R., Fayaz, K., Liu, B.J., 2021. Pd-based catalysts promoted by hierarchical porous Al_2O_3 and ZnO microsphere supports/coatings for ethyl acetate highly active and stable destruction. J. Hazard. Mater. 401, 123281.

Mazzarino, I., Barresi, A.A., 1993. Catalytic combustion of VOC mixtures in a monolithic reactor. Catal. Today 17, 335–347.

Novaković, T., Radić, N., Grbić, B., Marinova, T., Stefanov, P., Stoychev, D., 2008. Oxidation of *n*-hexane over Pt and Cu-Co oxide catalysts supported on a thin-film zirconia/stainless steel carrier. Catal. Commun. 9, 1111–1118.

Ordóñez, S., Bello, L., Sastre, H., Rosal, R., Díez, F.V., 2002. Kinetics of the deep oxidation of benzene, toluene, *n*-hexane and their binary mixtures over a platinum on gamma-alumina catalyst. Appl. Catal. B: Environ. 38, 139–149.

Papaefthimiou, P., Ioannides, T., Verykios, X.E., 1997. Combustion of non-halogenated volatile organic compounds over group VIII metal catalysts. Appl. Catal. B: Environ. 13, 175–184.

Papaefthimiou, P., Ioannides, T., Verykios, X.E., 1998. Performance of doped Pt/TiO_2 (W^{6+}) catalysts for combustion of volatile organic compounds (VOCs). Appl. Catal. B: Environ. 15, 75–92.

Qiao, B.T., Wang, A.Q., Yang, X.F., Allard, L.F., Jiang, Z., Cui, Y.T., Liu, J.Y., Li, J., Zhang, T., 2011. Single-atom catalysis of CO oxidation using Pt_1/FeO_x. Nat. Chem. 3, 634–641.

Qiao, B.T., Liang, J.X., Wang, A.Q., Xu, C.Q., Li, J., Zhang, T., Liu, J.J., 2015. Ultrastable single-atom gold catalysts with strong covalent metal-support interaction (CMSI). Nano Res. 8, 2913–2924.

Ribeiro, B.M.B., Pinto, J.F., Suppino, R.S., Marçola, L., Landers, R., Tomaz, E., 2019. Catalytic oxidation at pilot-scale: efficient degradation of volatile organic compounds in gas phase. J. Hazard. Mater. 365, 581–589.

Si, W., Wang, Y., Peng, Y., Li, X., Li, K., Li, J., 2015. A high-efficiency γ-MnO_2-like catalyst in toluene combustion. Chem. Commun. 51, 14977–14980.

Thang, H.V., Pacchioni, G., Rita, L.D., Christopher, P., 2018. Nature of stable single atom Pt catalysts dispersed on anatase TiO_2. J. Catal. 367, 104–114.

Venkateswarlu, G., Madhu, D., Rani, J.V., 2020. Graphene/β-MnO_2 composites–synthesis and its electroanalytical properties study in the Mg storage battery. Int. J. Energy Res. 44, 10238–10250.

Voisin, T., Erriguible, A., Aymonier, C., 2020. A new solvent system: hydrothermal molten salt. Sci. Adv. 6, eaaz7 770..

Wang, H., Xu, D.Y., Guan, E.J., Wang, L., Zhang, J., Wang, C.T., Wang, S., Xu, H., Meng, X.J., Yang, B., Gates, B.C., Xiao, F.S., 2020a. Atomically dispersed Ru on manganese oxide catalyst boosts oxidative cyanation. ACS Catal. 10, 6299–6308.

Wang, Z.W., Ma, P.J., Zheng, K., Wang, C., Liu, Y.X., Dai, H.X., Wang, C.C., His, H.C., Deng, J.G., 2020b. Size effect, mutual inhibition and oxidation mechanism of the catalytic removal of a toluene and acetone mixture over TiO_2 nanosheet-supported Pt nanocatalysts. Appl. Catal. B: Environ. 274, 118963.

Wu, J.C.S., Lin, Z.A., Pan, J.W., Rei, M.H., 2001. A novel boron nitride supported Pt catalyst for VOC incineration. Appl. Catal. A: Gen. 219, 117–124.

Wu, Y.S., Yuan, S.S., Feng, R., Ma, Z.C., Gao, Y.Z., Xing, S.T., 2017. Comparative study for low-temperature catalytic oxidation of *o*-xylene over doped OMS-2 catalysts: role of Ag and Cu. Mol. Catal. 442, 164–172.

Xiao, Y.C., Li, H., Xie, K., 2021. Activating lattice oxygen at the twisted surface in a mesoporous CeO_2 single crystal for efficient and durable catalytic CO oxidation. Angew. Chem. Int. Ed. 60, 5240–5244.

Xie, S.H., Deng, J.G., Zang, S.M., Yang, H.G., Guo, G.S., Arandiyan, H., Dai, H.X., 2015. Au–Pd/3DOM Co_3O_4: Highly active and stable nanocatalysts for toluene oxidation. J. Catal. 322, 38–48.

Xu, T.Z., Zheng, H., Zhang, P.Y., 2020. Isolated Pt single atomic sites anchored on nanoporous TiO_2 film for highly efficient photocatalytic degradation of low concentration toluene. J. Hazard. Mater. 388, 121746.

Yang, J., Hu, S.Y., Shi, L.M., Hoang, S., Yang, W.W., Fang, Y.R., Liang, Z.F., Pan, C.Q., Zhu, Y.H., Li, L., Wu, J., Hu, J.P., Guo, Y.B., 2021. Oxygen vacancies and lewis acid sites synergistically promoted catalytic methane combustion over perovskite oxides. Environ. Sci. Technol. 55, 9243–9254.

Yang, K., Liu, Y.X., Deng, J.G., Zhao, X.T., Yang, J., Han, Z., Hou, Z.Q., Dai, H.X., 2019a. Three-dimensionally ordered mesoporous iron oxide-supported single-atom platinum: highly active catalysts for benzene combustion. Appl. Catal. B: Environ. 244, 650–659.

Yang, M., Liu, J., Lee, S., Zugic, B., Huang, J., Allard, L.F., Flytzani-Stephanopoulos, M., 2015. A common single-site Pt(II)-$O(OH)_x$-species stabilized by sodium on "active" and "inert" supports catalyzes the water-gas shift reaction. J. Am. Chem. Soc. 137, 3470–3473.

Yang, X.Q., Yu, X.L., Lin, M.Y., Ma, X.Y., Ge, M.F., 2019b. Enhancement effect of acid treatment on Mn_2O_3 catalyst for toluene oxidation. Catal. Today 327, 254–261.

Yin, P.Q., Yao, T., Wu, Y., Zheng, L.R., Lin, Y., Liu, W., Ju, H.X., Zhu, J.F., Hong, X., Deng, Z.X., Zhou, G., Wei, S.Q., Li, Y.F., 2016. Single cobalt atoms with precise N-coordination as superior oxygen reduction reaction catalysts. Angew. Chem. Int. Ed. 55, 10800–10805.

Yuan, Z.B., Zhong, L.J., Lau, A.K.H., Yu, J.Z., Louie, P.K.K., 2013. Volatile organic compounds in the Pearl River Delta: Identification of source regions and recommendations for emission-oriented monitoring strategies. Atmos. Environ. 76, 162–172.

Zhang, J., Wu, X., Cheong, W.C., Chen, W., Lin, R., Li, J., Zheng, L., Yan, W., Gu, L., Chen, C., Peng, Q., Wang, D., Li, Y., 2018. Cation vacancy stabilization of single-atomic-site $Pt_1/Ni(OH)_x$ catalyst for diboration of alkynes and alkenes. Nat. Commun. 9, 1002.

Zhang, Y., Liu, Y.X., Xie, S.H., Huang, H.B., Guo, G.S., Dai, H.X., Deng, J.G., 2019. Supported ceria-modified silver catalysts with high activity and stability for toluene removal. Environ. Int. 128, 335–342.

Zhang, Y.H., 2018. In-situ IR study for elucidating the adsorption cracking mechanism of toluene over calcined olivine catalyst. Int. J. Hydrog. Energy 43, 15835–15842.

Zhang, Z., Zhu, Y., Asakura, H., Zhang, B., Zhang, J., Zhou, M., Han, Y., Tanaka, T., Wang, A., Zhang, T., Yan, N., 2017. Thermally stable single atom Pt/m-Al_2O_3 for selective hydrogenation and CO oxidation. Nat. Commun. 8, 16100.

Zhao, S.Z., Wen, Y.F., Liu, X.J., Pen, X.Y., Lü, F., Gao, F.Y., Xie, X.Z., Du, C.C., Yi, H.H., Kang, D.J., Tang, X.L., 2020. Formation of active oxygen species on single-atom Pt catalyst and promoted catalytic oxidation of toluene. Nano Res. 13, 1544–1551.

Zheng, J.Y., Yu, Y.F., Mo, Z.W., Zhang, Z., Wang, X.M., Yin, S.S., Peng, K., Yang, Y., Feng, X.Q., Cai, H.H., 2013. Industrial sector-based volatile organic compound (VOC) source profiles measured in manufacturing facilities in the Pearl River Delta. China Sci. Total Environ. 456–457, 127–136.

Zheng, Y.F., Liu, Q.L., Shan, C.P., Su, Y., Fu, K.X., Lu, S.C., Han, R., Song, C.F., Ji, N., Ma, D.G., 2021. Defective ultrafine MnO_x nanoparticles confined within a carbon matrix for low-temperature oxidation of volatile organic compounds. Environ. Sci. Technol. 55, 5403–5411.

Zhu, L.L., Shen, D.K., Luo, K.H., 2020. A critical review on VOCs adsorption by different porous materials: species, mechanisms and modification methods. J. Hazard. Mater. 389, 122102.